Radiochimica Acta *68*, 41–49 (1995)

Thermochromatographic Investigation of ^{13}N Labelled Nitrous Gases and of Fission Noble Gases at Low Temperatures

By B. Eichler, U. Baltensperger, M. Ammann, D. T. Jost, H. W. Gäggeler* and A. Türler
Paul Scherrer Institut, CH-5232 Villigen PSI, Switzerland

(Received July 25, 1994; revised August 29, 1994)

Thermochromatography / Adsorption enthalpy / Nitrogen dioxide / Nitrogen oxide / Nitric acid / ^{13}N / $^{138,139}Xe$

Abstract

A thermochromatographic device was developed which allows to study volatile species with deposition temperatures as low as 88 K.

With this device the adsorption behaviour of carrier free ^{13}NO, $^{13}NO_2$ and $H^{13}NO_3$ as well as of $^{138,139}Xe$ and ^{91}Kr on solid surfaces was investigated. As stationary phases the following materials were used: quartz, teflon, graphite, TiO_2, V_2O_5/TiO_2, and molecular sieve 5A.

From the experimentally measured deposition temperatures the differential molar adsorption enthalpies at zero coverage were determined.

The experiments clearly showed that thermochromatographic processes still lead to well defined chromatographic peaks even at temperatures as low as 88 K and high gas flow rates of 1 l/min.

Introduction

Thermochromatography, as a special form of gas adsorption chromatography, has found widespread applications for studying the adsorption behaviour of radionuclides and their compounds.

Separations in temperature gradient tubes have been reported for maximum temperatures of 2400 K, e.g. Y on Ta surfaces (adsorption enthalpy −627 kJ/mol) [1]. However, only very few measurements are reported for low temperatures. In a column kept – at the low temperature side – at 140 K the adsorption enthalpy of radon on palladium surfaces was determined to be (−37±4) kJ/mol [2].

The investigation of the adsorption behavior of gases at low temperatures is instrumental to understand cryogenic processes like the operation of a cold trap or the interaction of gases and aerosols in the upper atmosphere. Thermochromatography experiments at low temperatures can contribute thermochemical data, such as adsorption enthalpies, needed to describe adsorption reactions. In addition, thermochromatography allows fast separation of radionuclides and their compounds. Usually short-lived radionuclides are transported from the production site (reactor, cyclotron) to the laboratory with a gas-jet transportation system, therefore, the influence of high carrier gas velocities on the quality of the separation has to be investigated at the same time.

At low temperatures the limits of the operation principle of thermochromatography could be reached. Low diffusion coefficients and small sticking probabilities could prevent highly volatile compounds from being deposited in the chromatography column and from forming a typical adsorption peak. In the present study we investigated the formation of adsorption peaks at temperatures down to 90 K and carrier gas velocities up to 1 l/min. A comparison of the experimentally determined adsorption enthalpies with literature data, as well as model calculations with a Monte Carlo code, allow to check whether thermochromatography remains a powerful method even at very low temperatures.

Experimental

The device

Figure 1 shows a schema of the device. The temperature gradient along the column is produced by a metal tube (INCONEL 600). At one end of the tube a tubular oven is used to produce the maximum temperature and at the other end a liquid nitrogen cooling defines the minimum temperature. If the INCONEL tube is in direct contact with liquid nitrogen column temperatures below 100 K may be reached (version b in Fig. 1).

Fig. 2 depicts some examples of measured temperature profiles for a quartz column with different helium carrier gas flow rates. During these measurements heating and cooling were kept constant. It can be seen that different gas flow rates produce different temperature profiles.

During the experiments radioactive species were introduced with the carrier gas from the heated end into the column. At the low temperature side the carrier gas passed a cooled molecular sieve filter. Typical gas flow rates were on the order of 1 l/min.

Columns

Quartz tubes (i.d. 4 mm) were used as columns. As stationary phases the materials listed in Table 1 where

* *also at:* Institut für anorg. Chemie, Universität Bern, Freiestrasse 3, CH-3012 Bern, Switzerland.

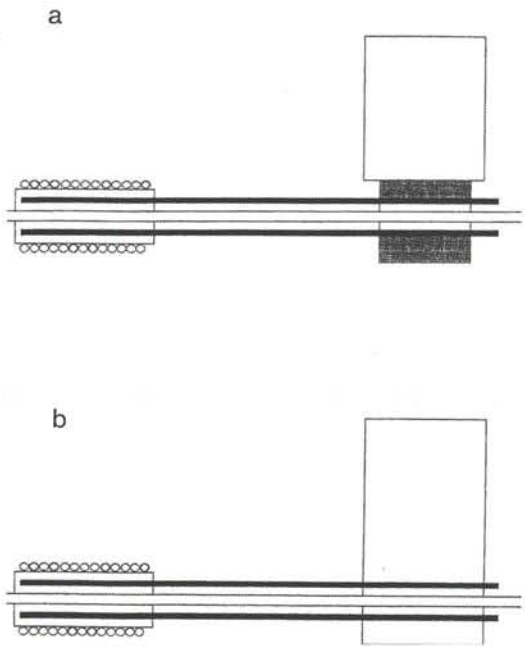

Fig. 1. Schema of the thermochromatographic device. a): copper contact cooling (T_{min} = 115 K); b): direct cooling with liquid nitrogen (T_{min} = 88 K).

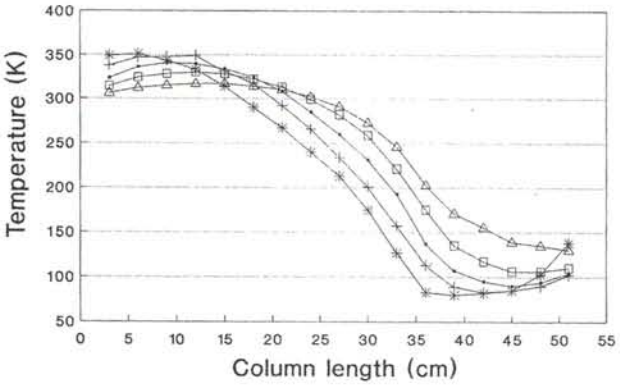

Fig. 2. Temperature profiles in an empty quartz column (type b) as a function of different gas flow rates. He gas flow (cm³/min): * stationary; + 600; • 1200; □ 2000; △ 4300.

Table 1. Characteristics of the quartz thermochromatography columns

Stationary phase	Surface area per unit length [cm²/cm]	Method for surface area determination
empty quartz column	1.2	calc*
quartz powder	10	calc*
V_2O_5/TiO_2	39700	BET
TiO_2	38700	BET
molecular sieve 5A	358000	BET
graphite fibres	40000	calc*
teflon rings	2.8	calc*
glass spheres	8.9	calc*

calc*: surface calculated from geometric dimensions.

filled into these quartz columns. From the specific surface and the total mass the surface area per unit length was determined.

Preparation of the radioactive gases

For the investigations at low temperatures ^{13}N labelled molecules such as NO, NO_2 and HNO_3 and the nuclear fission rare gases Xe and Kr were used.

^{13}N was produced in the reaction $^{16}O(p,\alpha)^{13}N$. A gas target of 70 mm length consisting of a mixture of 580 ml/min He and 100 ml/min O_2 was bombarded at the PSI PHILIPS cyclotron by 250 nA of 14 MeV protons [4]. The gas mixture containing the reaction products was transfered through a 2 mm i.d. polyethylene capillary over a distance of about 100 m to the thermochromatography device. The production of the different ^{13}N labelled species is described in detail in Ref. [4]: The primary product from the target chamber was mainly $H^{13}NO_3$, which was presumably formed with trace amounts of water vapour in the gas. HNO_3 was converted to NO using a molybdenum converter. Behind the molybdenum converter NO_2 was produced from NO by oxidation with chromium trioxide soaked with phosphoric acid. Addition of ozone to the NO resulted in formation of HNO_3, since concentrations of impurities such as H_2O were high compared to the ^{13}NO concentration (10^5 molecules per cm³ [4]).

The fission noble gases Xe and Kr were produced at the SAPHIR reactor gas-jet system [5]. As carrier gas 1 l/min He, without O_2, was used.

Recording of the chromatograms via radioactivity measurements

For the investigations of the fission noble gases the carrier gas was passed for two hours through the column. Then the column was removed and cut into 3 cm long pieces. The deposition peaks of ^{91}Kr ($T_{1/2}$ = 8.6 s), ^{138}Xe ($T_{1/2}$ = 14.1 min) and ^{139}Xe ($T_{1/2}$ = 39.7 s) were determined via measurement of the γ-spectra of their β-decay products ^{91}Sr ($T_{1/2}$ = 9.5 h), ^{138}Cs ($T_{1/2}$ = 32.2 min) and ^{139}Ba ($T_{1/2}$ = 1.38 h), respectively. This technique allowed to perform the γ-counting without cooling since these non-volatile daughters and grand-daughters of the rare gas radionuclides remained sorbed at the surface of the column material also at room temperature. The measurement of the 3 cm long column segments was performed with a high purity Ge detector.

The carrier gas containing the NO, NO_2 and HNO_3 molecules to be investigated was fed into the chromatography column for 20 min. Then the column was removed from the oven system, closed at both ends and put into an open bath of liquid nitrogen to freeze the distribution of the deposited gaseous species. The measurement of the γ-activity was performed with a Geiger-Müller counter using a lead collimator with a

3 cm slit. ^{13}N was detected via its 511 keV annihilation γ-rays.

Results and discussion

Distributions of HNO_3, NO_2, and NO in the thermochromatographic columns

Figures 3 and 4 show examples of measured distributions. Figs. 3a and 4a depict the temperature profiles. All plots are normalized, i.e. the sum of the measured count-rates for all 3 cm segments is 100%. Fig. 3b shows the measured distribution with the carrier gas containing the original composition of ^{13}N species behind the target chamber in a column filled with V_2O_5/TiO_2. Most of the activity is found at the entrance of the column which can be interpreted as an irreversible deposition of nitric acid. A minor part of the activity is found at lower temperatures. As will be discussed below, this fraction with higher volatility can most likely be attributed to NO.

A similar deposition pattern was observed with molecular sieve as stationary phase in experiments with HNO_3 (i.e. behind the molybdenum converter and adding ozone) (Fig. 4b).

Fig. 3c shows the measured distribution with pure NO (i.e. behind the molybdenum converter) for pure TiO_2. The highest peak can be attributed to NO. However, there is still a minor peak visible which can be attributed to NO_2. Since the molybdenum converter was shown to be more than 99% efficient (4) this NO_2 has to be assigned to oxidation on the column surface.

In case of a poor performance of the molybdenum converter, all three components are visible, as exemplified in Fig. 3d for a V_2O_5/TiO_2 filled column.

Fig. 3e shows the measured distribution for a NO_2 generator. The broad distribution clearly indicates that the conversion of NO to NO_2 is not quantitative. The same observation is made with the NO_2 generator fed into a molecular sieve column (Fig. 4c).

If the carrier gas containing all reaction products is fed into column filled with quartz powder, the products HNO_3 and NO_2 are observed whereas NO is absent (Fig. 4d). This highly volatile molecule can not be deposited under these conditions and is found in the following molecular sieve trap cooled with liquid nitrogen. The same result is found for an empty quartz column (Fig. 4e).

The method used in this work for the determination of the activity distributions led to an unrealistic broadening of the peak shapes. Therefore, in the following only the peak maxima will be discussed. They were converted to adsorption temperatures using the temperature pattern depicted in Figs. 3a and 4a.

Fig. 5 shows the distribution of xenon isotopes as it was recorded via the measurement of the daughter nuclides (see above). Since ^{138}Xe and ^{139}Xe have different half-lives, the deposition peaks have their maxima at slightly different adsorption temperatures. The shorter-lived isotope ^{138}Xe is – as expected – found

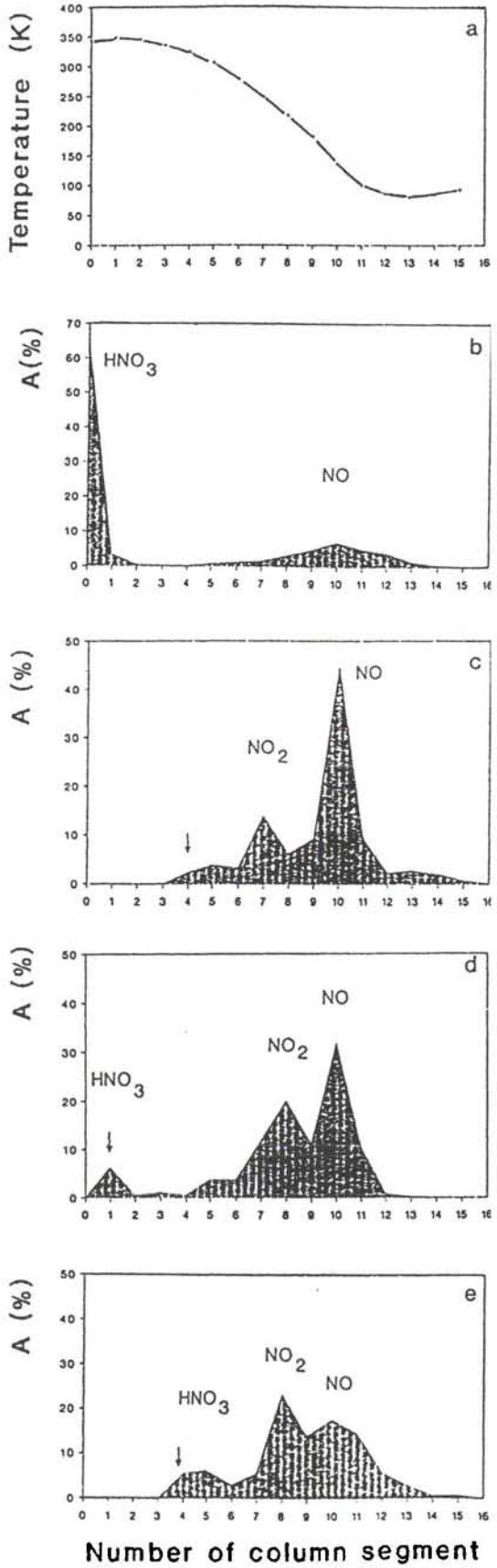

Fig. 3. Temperature along the column (a) and distribution of different mixtures of ^{13}N compounds in columns filled with V_2O_5/TiO_2 (b, d, e) and with TiO_2 (c) respectively; (↓ denotes the beginning of the column packing; length of column segment: 3 cm; A: relative part of the total activity in the column).

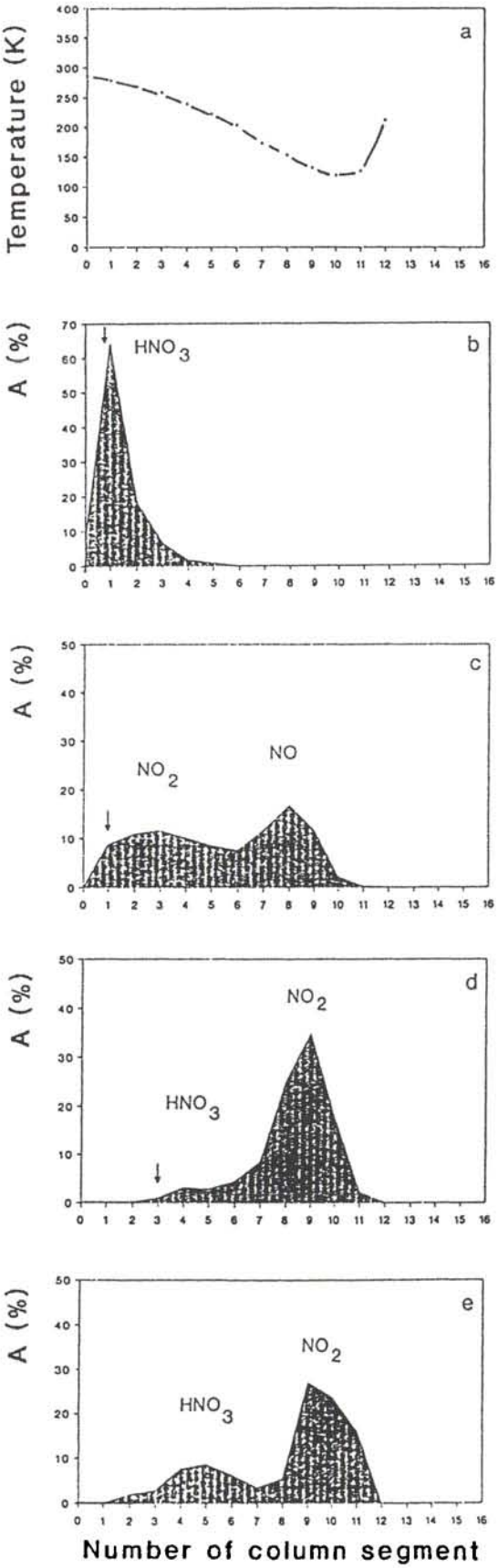

Fig. 4. Temperature along the column (a) and distribution of different mixtures of ^{13}N compounds in columns filled with molecular sieve (b, c), SiO_2 powder (d) and in an empty quartz column (e). (↓ denotes the beginning of the column packing; length of column segment: 3 cm; A: relative part of the total activity in the column).

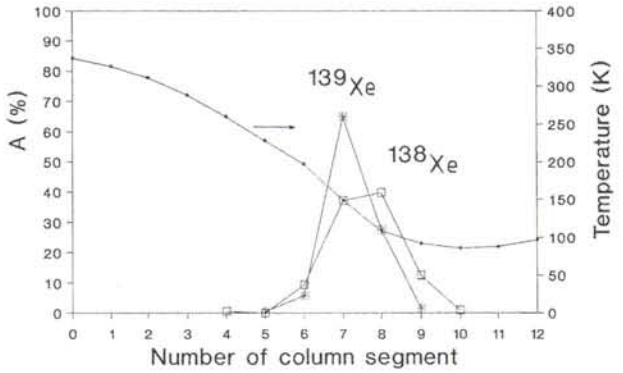

Fig. 5. Distribution of short-lived xenon isotopes in a thermochromatographic column filled with V_2O_5/TiO_2; (length of column segment: 3 cm, A: relative part of the total activity in the column).

at higher temperatures. In this column filled with V_2O_5/TiO_2 no decay products of ^{81}Kr were found.

Determination of adsorption enthalpies and intercomparison with literature data

Fig. 6 shows the relationship between the experimentally determined deposition temperatures T_d for NO, NO_2 and HNO_3 in the columns used and the parameter $\Delta Ei^*(x)$, which is described in [3] and includes experimental parameters as well as the adsorption entropy:

$$\Delta Ei^*(x) = \frac{t_r\, v_0\, g}{a T_0 \exp(\Delta S_a/R)} \tag{1}$$

with

t_r = duration of the experiment (retention time)
v_0 = gas flow rate
g = temperature gradient along the column
a = surface area of the column per unit length
ΔS_a = adsorption entropy
T_0 = standard temperature (273.15 K)
R = gas constant.

Mobile adsorption was assumed which allows to calculate ΔS_a [3]:

$$\Delta S_a = R \ln \tau_0 [RT_d/2\pi M]^{1/2} + R/2 \tag{2}$$

with

M = molecular weight
τ_0 = vibrational frequency of adsorbed species $[= 2.2 \cdot 10^{-13}\ \mathrm{s}]$.

The solid lines shown in Fig. 6 represent species with fixed adsorption enthalpies between -10 and -60 kJ/mol and deposition temperatures between 50 and 350 K, calculated with

$$\Delta Ei^*(x) = Ei^*\left(\frac{-\Delta H_a}{RT_d}\right) - Ei^*\left(\frac{-\Delta H_a}{RT_s}\right) \tag{3}$$

with

T_s = maximum temperature in the column
ΔH_a = adsorption enthalpy.

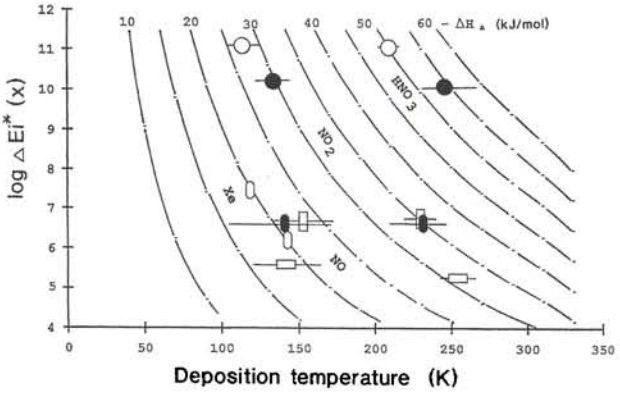

Fig. 6. Parameter $\Delta Ei^*(x)$ (solid lines) for selected values of $-\Delta H_a$ (10 ... 60 kJ/mol) as function of deposition temperature T_d according to Eq. (3).
Included are the average experimental deposition temperatures in various columns at accompanying values of $\Delta Ei^*(x)$ from Eq. (1). ○ empty quartz tube; ● quartz powder; ◖ V_2O_5/TiO_2; ▯ TiO_2; ▭ molecular sieve; ◊ Xe on V_2O_5/TiO_2.

Table 2. Parameter $Ei^*(x)$ (see text) and lowest detectable adsorption enthalpies ΔH_a for minimum temperatures of 115 K and 88 K, respectively, for the columns used in this work

Column type	$\Delta Ei^*(x)$	$-\Delta H_{a\,min}$ (kJ/mol) $T_{d\,min}$ = 115 K	$-\Delta H_{a\,min}$ (kJ/mol) $T_{d\,min}$ = 88 K
Empty quartz tube	1.7×10^{11}	27.5	21.3
Filled quartz tube	2.0×10^{10}	25.8	19.7
V_2O_5/TiO_2	7.0×10^{6}	17.8	13.7
Molecular sieve	5.8×10^{5}	15.2	11.7

The experimentally determined ΔEi^* values for a given species form for each column type a set of data which are grouped in the two dimensional plot (different symbols in Fig. 6).

Given by the minimum temperature and the gas flow rate in the thermochromatography apparatus for each column type a lower limit of the adsorption enthalpy is defined by Eq. (3). For the columns and the retention times used in this work the minimum detectable adsorption enthalpies are summarized in Table 2.

The calculated lower limits were confirmed experimentally. As an example, in empty quartz columns or in columns filled with non-porous materials NO was not deposited at the minimum temperatures achieved in this work. The same holds for Kr.

In all investigations non-deposited species (e.g. ^{13}NN) were adsorbed in the molecular sieve traps cooled with liquid nitrogen and were also measured [4].

For an estimate of the adsorption enthalpies the following empirical correlation was applied, which can be used for (non-strongly selective chemical) sorption of non-basic oxides and hydroxides on quartz surfaces [6]:

$$-\Delta H_a = [16.9 \pm 8.2] + [0.690 \pm 0.042] \cdot \Delta H_{subl} \quad (4)$$

Table 3. Sublimation enthalpies and estimated adsorption enthalpies for different species on quartz surface. For comparison the sublimation enthalpies of some elements are added

Species	Sublimation enthalpy [7] [kJ/mol]	Adsorption enthalpy (from (Eq. (4)) [kJ/mol]
NO	16.07	28.0± 8.9
NO_2	51.00	52.0±10.3
HNO_3	49.70	51.2±10.3
N_2	6.31	–
O_2	7.28	–
Kr	10.69	–
Xe	14.92	–

Table 3 summarizes the calculated adsorption enthalpies obtained with Eq. (4) using literature values of the sublimation enthalpies [7].

Table 4 summarizes adsorption enthalpies of NO, NO_2 and HNO_3 from the literature and from this work. The assignment to isosteric, differential or integral adsorption enthalpy is made according to the corresponding references [10–41].

Under the actual experimental conditions of the thermochromatography experiment, not the adsorption of the investigated species on the clear column surface was studied, but the co-adsorption of nitrogen oxides or fission noble gases with other components and impurities (e.g. H_2O, CO_2) of the carrier gas. The rather high gas flow velocities – which are mandatory for a fast transport of short-lived nuclides – might, however, influence the deposition process. Especially at low temperatures with low diffusion velocities it can not entirely be excluded that kinetic effects might prevent a full adsorption equilibration. In helium the diffusion coefficients decrease by approximately one order of magnitude if the temperature is lowered from room temperature to 100 K [9]. Hence, the measured deposition temperatures in open tubes and in loosely packed tubes could yield too low adsorption enthalpies. The thermochromatography does not allow to determine adsorption enthalpies on the basis of mere thermodynamic relationships [3]. The analysis is based on the assumption of an adsorption model which also includes a prediction of the adsorption entropy. Hence, only approximations of the adsorption enthalpy can be obtained. The result is a differential molar adsorption enthalpy under zero coverage. The values obtained can be compared with isosteric and differential adsorption enthalpies at zero coverage, obtained with other, conventional techniques. Comparison with integral adsorption enthalpies at very low coverage is also possible. For higher coverages isosteric and differential adsorption enthalpies can only be compared if the coverages are the same. This is especially important for nitrogen oxides which tend to associate (e.g. $2\,NO_2 \leftrightarrow N_2O_4$).

The large scatter of the existing literature data only allows to define an approximate differentiation of the

Table 4. Adsorption enthalpies of NO, NO_2 and HNO_3-corresponding references

Adsorbent	Method	Temp. (K)	Coverage	$-\Delta H_a$ (kJ/mole)			Reference *denotes this work
				isosteric	integral	differential	
			NO				
SiO_2 tube	tc	<115	zero			<28	*
SiO_2 powder	tc	<115	zero			<26	*
glass spheres	tc	90–130	zero			18.0±0.5	*
Silica	gr		0.4–1.0	9...16			10
Cab–O–Sil							
MgO	vo	70–150	0.1	23.0			11
MgO	vo	243–303	0.02	16.7			12
Al_2O_3	gr		0.5	8.0			13
Al_2O_3	gr	181–273				16.7–20.9	14
SnO_2				37.6			15
KCl	ma	88–113	0.07	15.5			16
			0.007	17.8			
Mordenite:							
H-mordenite	vo	213–343	0.02	23.4			17
H-ZSM mordenite	vo	213–343	0.02	18.4			17
Li-mordenite	vo	213–388	0.02	31.5			18
Na-mordenite	vo	213–388	0.02	27.6–30.1			18
Na-mordenite	vo	243–303	0.02	29.7–27.6			12
K-mordenite	vo	213–388	0.02	22.6			18
Cs-mordenite	vo	213–388	0.02	20.9			18
natural mordenite	gc	133–261	zero			20.1	20
Mg-mordenite	ma		0.02		41–63		19
Ca-mordenite	ma		0.02		38–41		19
Ba-mordenite	ma		0.02		33		19
Molecular sieves:							
5A	gc	210–261	zero			37.2	20
5A	tc	130–170	zero			18.6±2.7	*
13X	gc	133–261	zero			18.2	20
Carbon:							
activ.	vo	200			29.5		21
chercol		230			33.0		
		270			36.8		
activ.	vo	273				30.0	22
coal		313				31.1	
Sterling	gr		0.8	12.0			10
FT			1.0	18			
ungrap. carbon	gr			16.6			10
graphit	ca		zero			200	23
graphit	ca	190–273		4.0			24
graphit	tc	135–318	zero			20.3±1.0	*
Oxides of transit. metals:							
TiO_2	tc	138–183	zero			23.2±2.2	*
V_2O_5/TiO_2	tc	125–150	zero			19.3±2.2	*
$V_2O_5/TiO_2(NH_3)$	tc	130–166	zero			23.1±2.2	*
Cr_2O_3/Al_2O_3	gr	≤373	0.3–0.4	23.0			25
			0.1		48.2		
CrO/SiO_2	ca					126	26
$LaCrO_3$	vo	195–301	0.5		40		27
$LaFeO_3$	vo	195	0.65–1.0			25–38	28
Fe_2O_3/Al_2O_3	gc	643–683	zero			50.2	29
Fe_2O_3	gr	299–423	0.37		23.0		30
NiO	gr		0.5	6			13
NiO		181–286			20.0		32
NiO	gr	273–413	0.37	36.0			33

Table 4. (Continued).

Adsorbent	Method	Temp. (K)	Coverage	$-\Delta H_a$ (kJ/mole)			Reference *denotes this work
				isosteric	integral	differential	
			NO_2				
SiO_2 tube	tc	108–120	zero			27.4±2.7	*
SiO_2 powder	tc	127–148	zero			29.7±2.5	*
glass spheres	tc	90–130	zero			22.0±1.5	*
Mordenite:							
natural-mordenite	gc	133–261	zero			10.0	20
H-mordenite	gc	133–261	zero			10.0	20
Na-mordenite	gc	210–261	zero			12.1	20
Mo-glass	vo	393–523			11.5		38
carb.fibres ACF	gr	566–626				40–77	39
graphit	tc	234–318	zero			35.2±2.5	*
Teflon	tc	121–318	zero			27.5±2.5	*
Molecular sieves:							
5A	gc	131–261	zero			18.3	20
5A	tc	243–260	zero			31.6±1.0	*
13X	gc	133–261	zero			18.	20
TiO_2	tc	218–238	zero			34.6±1.5	*
$V_2O_5/TiO_2(NH_3)$	tc	218–230	zero			35.6±3.1	*
V_2O_5/TiO_2	tc	218–243	zero			34.5±1.5	*
Fe_2O_3	vo	393–523			12.8		38
Co_2O_3	vo	339–523			16.3		38
			HNO_3				
SiO_2 tube	tc	248	zero		(50.4)	*	
SiO_2 powder	tc	230–263	zero			53.7±3.0	*
Mol. sieve 5A	tc	573	zero			(78)	*
			Xe				
Graphit:							
Sterling MT 3100	ra	162–195	zero	20.1			40
Graphon	ra	162–195	zero	21.3			40
Molecular sieve:							
5A	ma	195–298				22.0	41
13X						22.0	41
AW-500						27.6	41
V_2O_5/TiO_2	tc	130–160				19.8	*
			Kr				
MS-5A	ma	195–298				15.6	41
MS-13X						14.6	41
V_2O_5/TiO_2	>88					<13.7	

Remarks: vo: volumetric; ma: manometric; gr: gravimetric; gc: gas chromatographic; tc: thermochromatographic; tpd: temperature programmed desorption; ra: radiometric; A/B: A supported on B.

adsorption properties as a function of the nature of the solid surfaces. It can be assumed that dimerization, disproportionation, surface oxidation and other irreversible processes strongly influence the experimental results.

On the adsorbent materials SiO_2, mordenites, molsieve, graphite, MgO and Al_2O_3 the molecule NO seems to be similarly adsorbed. Our experimental thermochromatographic data for ^{13}NO on graphite and molecular sieve 5 A fit well to this group.

Within the transition metal oxides increasing adsorption enthalpies are observed from TiO_2 to CuO. This indicates increasing chemical interaction of NO with the solid surface (possibly nitrosyl formation). Strongest adsorption is found for surfaces of mixed oxides with spinel structure [30, 37].

Our results for the adsorption of NO on TiO_2 and V_2O_5/TiO_2 catalytic materials are similar to literature values for the adsorption of NO on single transition metal oxides. When V_2O_5/TiO_2 was pretreated with ammonia a higher adsorption enthalpy for NO was found compared to untreated material. Possible reasons might be a modification of the chemisorption as well as a blocking of certain adsorption sites [4].

The studies with NO_2 were performed at a concentration level which did not allow formation of N_2O_4. However, most literature data for NO_2 sorption were made at temperatures where formation of N_2O_4 can be assumed [38, 39]. The scarce number of literature data does not allow a systematic interpretation with respect to different adsorbents.

It is surprising that for some materials the literature values for the adsorption enthalpies of NO are higher than for NO_2. This is in contrast to gas chromatographic studies [42] which clearly show that NO has lower deposition temperatures, and thus should be more volatile than NO_2, as expected on the basis of the corresponding sublimation enthalpies (see Table 6). Even if adsorption of N_2O_4 is assumed the dissociation of this molecule should not lower the adsorption enthalpy to values as low as 10 kJ/mol, as e.g. published for NO_2 on mordenite (see Table 4).

Gaseous nitric acid can be studied chromatographically on pure quartz surfaces only. On all other materials used in this work, irreversible adsorption with e.g. nitrate formation or decomposition occurred.

The investigation of the sorption behaviour of noble gases was made for calibration purposes. In general, only small variations of the adsorption enthalpies are found for different sorption materials. On the basis of the sublimation enthalpies (Table 6), for NO and Xe similar adsorption enthalpies are expected. The deposition of Xe defines physisorption. The rather similar experimental adsorption enthalpies for NO and Xe show that chemical interactions of NO with the oxides is of minor importance.

Calculation of thermochromatographic deposition zones using a Monte Carlo model

In order to achieve a better understanding on how the experimental conditions influence the formation of a deposition zone, a suitable model for gas-solid thermochromatography in open columns must be applied. However, severe difficulties are encountered in attempting to derive the zone shape analytically. Therefore, a microscopic model describing the erratic downstream migration of a gaseous species through an open column with a negative longitudinal temperature gradient is required. Since an exact model, simulating the vast number of adsorption-desorption cycles followed by intermittent displacements of each species, requires far too much computer time, the physical picture of these migrations must be simplified. Such a model was developed by Zvara [43]. The many adsorption-desorption cycles that result in a negligible longitudinal displacement of the species are combined in an adsorption residence event followed by an effective displacement. All parameters for the probability density distributions in the model have been adjusted so that the model adequately reflects the retention of the species in the system. This microscopic model has the advantage that it can accommodate the exact, measured temperature profiles as well as high carrier gas flow rates.

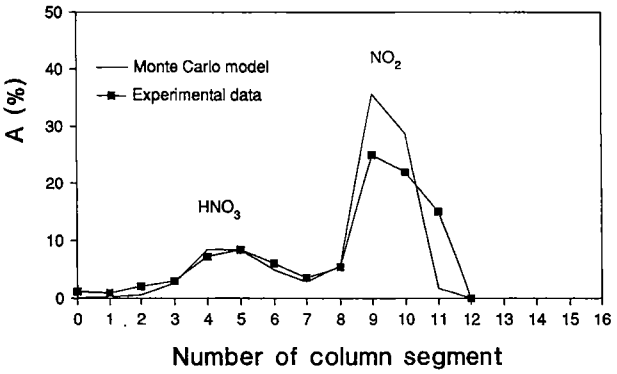

Fig. 7. Deposition zones of HNO_3 and NO_2 in an empty thermochromatographic column (data points) and the calculated distribution using a Monte Carlo model (line) at a carrier gas flow rate of 600 ml/min and adsorption enthalpies of −55 kJ/mol and −30 kJ/mol for HNO_3 and NO_2, respectively; (length of column segment: 3 cm; A: relative part of the total activity in the column).

We have applied this model to reproduce the observed deposition zones in the experiment depicted in Fig. 4e. The total activity in the column is distributed between $H^{13}NO_3$ (30%) and $^{13}NO_2$ (70%). The result of the Monte Carlo model calculation is shown in Fig. 7. Adsorption enthalpies of −55 kJ/mol and −30 kJ/mol were used for $H^{13}NO_3$ and $^{13}NO_2$, respectively. The deposition zones that result for $H^{13}NO_3$ and $^{13}NO_2$ contain each the statistics of 10000 simulated molecules. The agreement between calculated and observed deposition zones is excellent. In addition, the calculation revealed that all of the ^{13}NO (assuming an adsorption enthalphy of −20 kJ/mol) and also about 43% of the $^{13}NO_2$ molecules pass through the column without being deposited. The reason for this behavior is, that the end of the column is not cold enough to allow the deposition of all the molecules. Since the calculated deposition zones react very sensitive to changes in temperature in the coldest section of the column, small deviations from the measured temperature profile in the actual experiment may explain why the data point in segment 11 of the $^{13}NO_2$ deposition zone was not reproduced very well in the model calculation.

So far this model can be applied only for gas-solid chromatography in open columns.

Conclusions

Thermochromatography with carrier-free radionuclides can be used to study the adsorption behaviour for temperatures as low as 88 K. This corresponds to adsorption enthalpies of about 19 kJ/mol.

This allows applications in analytical as well as in preparative radiochemistry. Physico-chemical measurements allow investigations of gaseous species on solid surfaces at zero coverage. This method is applicable e.g. to heterogeneous catalysis with radiolabelled compounds.

The basic assumptions made and the model used for the interpretation of the data allow a prediction of the adsorption behaviour of species with even lower adsorption enthalpies.

Thus a preparative separation of Kr and Xe should be possible in a thermochromatographic column filled with molsieve.

References

1. Beyer, G.-J., Novgorodov, A. F., Khalkin, V. A.: Radiokhimija **20**, 589 (1978).
2. Eichler, B., Kim Son Chun: Isotopenpraxis **21**, 180 (1985).
3. Eichler, B., Zvara, I.: Radiochim. Acta **30**, 233 (1982).
4. Baltensperger, U., Ammann, M., Bochert, U. K., Eichler, B., Gäggeler, H. W., Jost, D. T., Kovacs, A., Türler, A., Scherer, U. W., Baiker, A.: J. Phys. Chem. **97**, 12325 (1993).
5. Ya Nai-Qi, Jost, D. T., Baltensperger, U., Gäggeler, H. W.: Radiochim. Acta **47**, 1 (1989).
6. Eichler, B., Domanov, V. P.: J. Radioanal. Nucl. Chem. **28**, 143 (1975).
7. Efimov, A. J.: *Svoistva Neorgasniceskikh Soedinienie*, Izd. Khimija, Leningrad 1983.
8. Maynard, V. R., Grushka, E.: Measurements of diffusion coefficients by gas chromatographic broadening techniques: A Review, p. 100 in: *Advances in Chromatography, Vol. 12*, Ed. Giddings J. C.; Marcel Dekker, Inc. New York (1975).
9. Andrussow, L.: in: *Landolt-Boernstein, Eigenschaften der Materie in ihren Aggregatszuständen, 5. Teil, Band a: Transportphänomene I*, Ed. K. Schäfer, Springer Verlag, Berlin (1969).
10. Brown, C. E., Hall, P. G.: J. Colloid Interface Sci. **42**, 334 (1973).
11. Furuyama, S., Fujii, H., Kawamura, M., Morimoto, T.: J. Phys. Chem. **82**, 1028 (1978).
12. Furuyama, S., Morimoto, T.: J. Phys. Chem. **82**, 1748 (1978).
13. Brown, C. E., Hall, P. G.: Surface Sci. **36**, 569 (1973).
14. Solbakken, A., Reyerson, L. H.: J. Phys. Chem. **64**, 1903 (1960).
15. Solimosi, F., Kiss, J.: Magy. Kem. Foly **81**, 450 (1975).
16. Granville, A., Hall, P. G.: J. Phys. Chem. **70**, 937 (1966).
17. Furuyama, S., Miyazaki, M., Inoue, H.: J. Phys. Chem. **88**, 1741 (1984).
18. Furuyama, S., Sato, K.: J. Phys. Chem. **86**, 2498 (1982).
19. Furuyama, S., Nagato, M.: J. Phys. Chem. **88**, 1735 (1984).
20. Yi Hua Ma, Maucel, C.: AiChE Journal **18**, 1148 (1972).
21. Hanono, F., Lerner, F.: J. Catal. **51**, 398 (1978).
22. Gregg, S. J.: J. Chem. Soc. 1494 (1927).
23. Zarifyants, Y. A.: Zh. Fiz. Khim. **38**, 643 (1964).
24. Cascarini De Tore, L. E., Arvia, A. J.: An. Quim. **64**, 349 (1968).
25. Otto, K., Shelef, M.: J. Catal. **14**, 226 (1969).
26. Della Gatta G., Fubini, B., Ghiotto, G., Giamello, E., Venturello, G.: J. Calorim. Anal. Therm. **9A** (A6), 49 (1978).
27. Olivian, A. M. O., Pena, M. A., Gonzales, L., Tenjuja: J. Molec. Catal. **45**, 355 (1988).
28. Pena, M. A., Tascon, J. M. D., Tejuca, L. G.: Nouv. J. Chim. **9**, 591 (1985).
29. Nijyama, H., Smith, J. M.: J. Catal. **41**, 359 (1976).
30. Otto, K., Shelef, M.: J. Catal. **18**, 1181 (1970).
31. Alexeyev, A., Terenin, A.: J. Catal. **4**, 440 ((1965).
32. Solbakken, A., Reyerson, H.: J. Phys. Chem. **64**, 2930 (1971).
33. Ghandi, H. S., Shelef, M.: J. Catal. **24**, 241 (1972).
34. Platero, E. E., Fubini, B., Zecchina, A.: Surface Sci. **179**, 404 (1987).
35. Ghandi, H. S., Shelef, M.: J. Catal. **28**, 1 (1973).
36. Udovic, T. J., Dumesic, J. A.: J. Catal. **89**, 314 (1984).
37. Yao, H. C., Shelef, M.: J. Phys. Chem. **78**, 2490 (1974).
38. Lurje, B. A., Seregin, V. V., Savin, A. M., Svetlov, B. S.: Zh. Fiz. Khim. **58**, 231 (1984).
39. Chupalev, V. S.: Zh. Prikl. Khim. (Leningrad) **56**, 2595 (1983).
40. Cochrane, H., Walker, P. L., Diethorn, W. S., Fridman, H. C.: J. Coll. Interface Sci. **24**, 405 (1967).
41. Kitani, S., Takada, J.: J. Nucl. Sci. Technol. **2**, 51 (1965).
42. Lawson, A., McAdie, H. G.: J. Chromatogr. Sci. **8**, 731 (1970).
43. Zvara, I.: Radiochim. Acta **38**, 95 (1985).